Anisotropic anomalous Hall effect in triangular itinerant ferromagnet Fe_3GeTe_2

Yihao Wang,[1,2] Cong Xian,[1,2] Jian Wang,[1,3] Bingjie Liu,[1,2] Langsheng Ling,[1] Lei Zhang,[1,2] Liang Cao,[1,2] Zhe Qu,[1,2,*] and Yimin Xiong[1,2,4,†]

[1]*Anhui Province Key Laboratory of Condensed Matter Physics at Extreme Conditions, High Magnetic Field Laboratory of the Chinese Academy of Sciences, Hefei, Anhui 230031, China*

[2]*University of Science and Technology of China, Hefei, Anhui 230026, China*

[3]*School of Physics and Material Science, Anhui University, Hefei, Anhui 230601, China*

[4]*Collaborative Innovation Center of Advanced Microstructures, Nanjing, 210093, China*

(Received 20 May 2017; revised manuscript received 22 August 2017; published 26 October 2017)

Magnetic frustrated materials are of great interest for their novel spin-dependent transport properties. We report an anisotropic anomalous Hall effect in the triangular itinerant ferromagnet Fe_3GeTe_2. When the current flows along the *ab* plane, Fe_3GeTe_2 exhibits the conventional anomalous Hall effect below the Curie temperature T_c, which can be depicted by Karplus–Luttinger theory. On the other hand, the topological Hall effect shows up below T_c with current along the *c* axis. The enhancement of Hall resistivity can be attributed to the chiral effect during the spin-flop process.

DOI: 10.1103/PhysRevB.96.134428

I. INTRODUCTION

The anomalous Hall effect (AHE) is a common phenomenon in ferromagnetic (FM) materials. It is generally accepted that two terms contribute to the AHE: one is induced by the Lorentz force, and the other is caused by the spin-orbit interaction (SOI) [1]. Thus, the Hall resistivity ρ_{xy} can be described by an empirical formula [2]

$$\rho_{xy} = R_0\mu_0 H + R_s M, \tag{1}$$

where R_0 and R_s represent the ordinary and anomalous Hall coefficients, respectively. The AHE is not only observed in ferromagnets but can also appear in materials which show large localized magnetic moment, such as strongly paramagnetic (PM) or antiferromagnetic (AFM) metals [2]. Recently, attention has been paid to magnetic frustrated materials exhibiting the topological Hall effect (THE), such as $PdCrO_2$ and $Fe_{1.3}Sb$ with a triangular lattice [3,4], $Pr_2Ir_2O_7$ and $Nd_2Mo_2O_7$ with a pyrochlore lattice [5,6], Mn_3Sn and Mn_3Ge with a Kagomé lattice [7–10], and antiferromagnets with noncollinear spin structures [11–13]. In these materials, the anomalous Hall resistivity is not proportional to magnetization, which cannot be explained by conventional AHE mechanisms, including Karplus–Luttinger (K-L) theory [14], skew scattering [15,16], and side jump [17]. As a consequence, Berry-phase-related mechanisms are developed, which in turn are adopted to explain the THE in magnetic frustrated materials [18–23].

The archetypal example of magnetic frustrated systems is AFM interacting spins in a triangular lattice. When two of the spins are pairwise anti-aligned, the remaining one cannot point in a direction that satisfies AFM interactions simultaneously with the former two spins, which gives rise to a large degeneracy of the system ground states [24,25]. Therefore, the spins in magnetic frustrated materials tend to form noncoplanar textures; namely, spin chirality, which endows the conduction electrons with a phase factor and acts as a fictitious magnetic field that leads to the THE [19–21,26]. However, because the fictitious magnetic field over the whole lattice sites generally balances out [27,28], the THE is not a common feature among magnetic frustrated materials. Consequently, searching for materials exhibiting the THE will contribute to understanding and verifying the THE mechanisms.

Fe_3GeTe_2 has a hexagonal crystal structure with a space group $P6_3/mmc$ [29], and is known as a quasi-two-dimensional (quasi-2D) itinerant ferromagnet with a Curie temperature T_c ranging from 150 to 220 K that depends on the Fe concentration [30]. There are triangular lattices formed by iron atoms and are parallel to the *c* axis, indicating that frustrated structure exists in Fe_3GeTe_2. Large susceptibility anisotropy has been reported with the magnetic field along the *c* axis and the *ab* plane [31], respectively. Moreover, recent magnetic measurements reveal a competing AFM state along the *c* axis [32]. As the temperature cools from 300 to 2 K, the ground states along the *c* axis vary successively from PM to AFM coexisting with FM, then to AFM. Whereas in the *ab* plane, the ground states vary from PM to FM [32]. All the results above remind us that Fe_3GeTe_2 may be a good candidate to investigate the THE.

In this study, we grew Fe_3GeTe_2 single crystals and performed transport measurements. Obvious magnetization and electronic transport anisotropy was observed. In particular, we found a THE in Fe_3GeTe_2 with current along the *c* axis. The Hall resistivity shows strong enhancement at low field below the Curie temperature. This behavior sharply contrasts with the behavior expressed by aforementioned empirical formula, and can be explained by chiral effect in magnetic frustrated material.

II. EXPERIMENTAL DETAILS

Single crystals of Fe_3GeTe_2 were grown by the chemical vapor transport method, referring to procedures described in the literature [31]. To get large single crystals for transport measurements, the transport agent I_2 is replaced by $TeCl_4$. The structure was characterized by x-ray diffraction

*zhequ@hmfl.ac.cn
†yxiong@hmfl.ac.cn

(XRD) analysis with Cu K_α radiation at room temperature by using a diffractometer (Rigaku-TTR3). Magnetic and electrical transport measurements were carried out by using a Quantum Design 7 T Magnetic Property Measurement System (SQUID-VSM3) and an Oxford Instrument TeslatronPT cryogenic system with the dc four-probe method, respectively. High-quality plate-like single crystals were used for these measurements to minimize the misalignment of samples. Both top and bottom surfaces of the samples are flat and parallel with each other. Before transport measurements, calibration of angle was performed to reach the best precision of experiments. All experiments were repeated to verify that the error from misalignment of sample mounting is negligible. For the measurement of magnetoresistance and Hall resistivity, single crystals were cut into rectangles with dimensions of $2 \times 1.5 \times 0.15$ mm^3. Details about transport measurements are given in Part I of the supplementary material [33]. To eliminate misalignment of electrodes, the resistivity and Hall resistivity were measured at both positive and negative fields.

III. RESULTS AND DISCUSSION

The crystal structure of Fe_3GeTe_2 is depicted in Figs. 1(a) and 1(b). Layered Fe_3Ge substructures are sandwiched by two layers of Te atoms with a van der Waals bond between adjacent Te layers. Within the substructure, seven Fe atoms share one vertex, forming three regular triangles, which imply that the frustrated feature exists in this material. Figure 1(c) shows the XRD pattern of a Fe_3GeTe_2 single crystal. Only the (00l) Bragg peaks are observed, demonstrating that the exposed

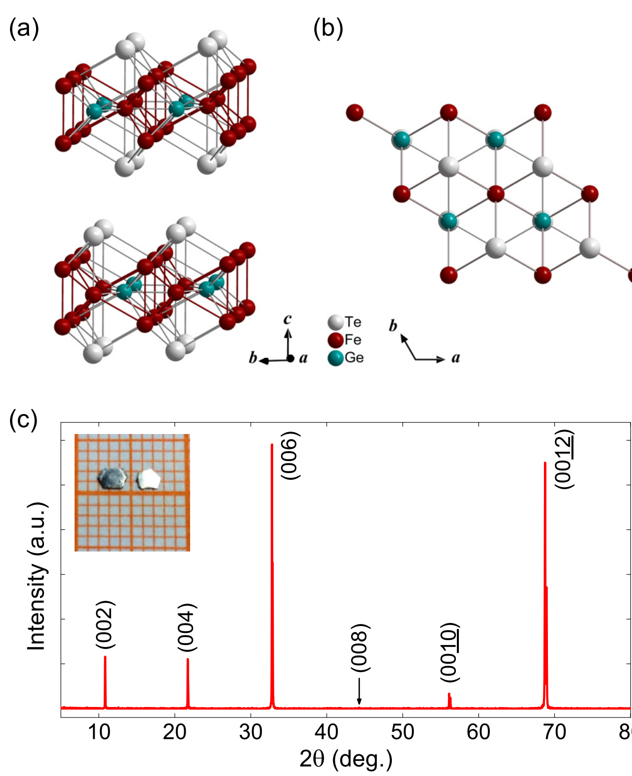

FIG. 1. (a) Crystal structure of Fe_3GeTe_2. (b) Top view of Fe_3GeTe_2. (c) XRD pattern of Fe_3GeTe_2 single crystal. The inset shows a photograph of Fe_3GeTe_2 single crystals on a 1 mm grid.

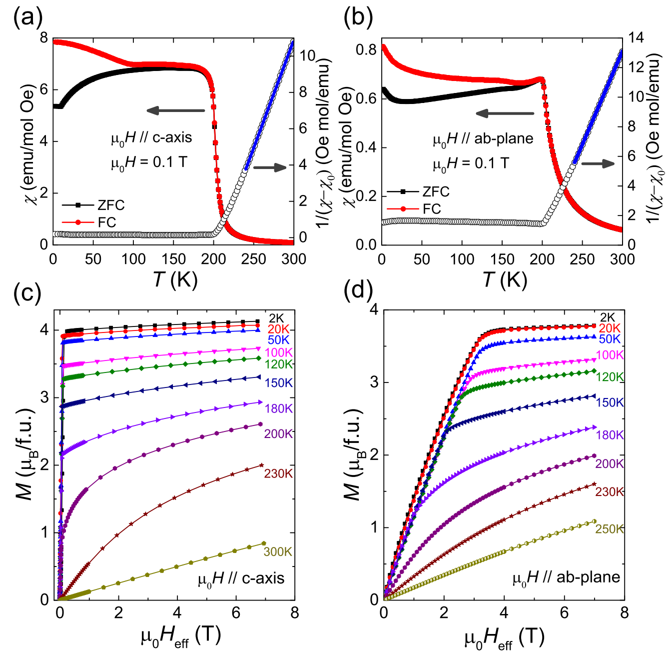

FIG. 2. (a), (b) Temperature dependence of susceptibility χ (left ordinate) and $1/(\chi - \chi_0)$ vs T behavior (right ordinate) with $H \parallel c$ axis and $H \parallel ab$ plane. The solid line indicates the fit with the modified Curie–Weiss law for temperatures ranging from 240 to 300 K. (c), (d) Field dependence of magnetization at indicated temperatures with $H \parallel c$ axis and $H \parallel ab$ plane.

surface is ab plane. The lattice parameter along the c axis is estimated to be 16.376 Å by using Bragg's law, which is consistent with reported values [29–31]. The inset of Fig. 1(c) shows two pieces of Fe_3GeTe_2 single crystals on a 1 mm grid. A typical crystal size is $2 \times 2 \times 0.15$ mm^3 with a hexagonal plate-like shape.

To understand the magnetic properties of Fe_3GeTe_2, temperature dependence of susceptibility χ is measured at 0.1 T and shown in Figs. 2(a) and 2(b). Rapid upturns are observed at 201 K for the field along the c axis ($H \parallel c$ axis) and 196 K for a field along the ab plane ($H \parallel ab$ plane), which demonstrates magnetic transitions occur at these temperatures [31]. Below the transition temperature, the susceptibility χ_c for $H \parallel c$ axis is about ten times larger than χ_{ab} for $H \parallel ab$ plane, which is in accord with reported data and indicates the anisotropic magnetic property in Fe_3GeTe_2 [31,32]. The $1/(\chi - \chi_0)$ vs T curves above 240 K can be fit by a modified Curie–Weiss law,

$$\chi(T) = \chi_0 + \frac{C}{T - \theta_p}, \qquad (2)$$

where χ_0 is a T-independent contribution to $\chi(T)$, C is the Curie constant, and θ_p is the Weiss temperature. The fits over the temperature ranging from 240 to 300 K using Eq. (2) are shown as solid blue curves in Figs. 2(a) and 2(b). The parameters χ_0, C, and θ_p obtained from the fits are listed in Table I. The effective moment derived from the fits is $4.74\mu_B$/Fe for $H \parallel c$ axis and $4.59\mu_B$/Fe for $H \parallel ab$ plane, which are consistent with literature values [31] and close to the theoretical value of $4.90\mu_B$/Fe for free Fe^{+2} ions with spin $S = 2$. This result indicates that all Fe ions in Fe_3GeTe_2 crystals

TABLE I. FM ordering temperatures obtained from $1/(\chi - \chi_0)$ vs T data and the parameters obtained from fits of the $1/(\chi - \chi_0)$ vs T data for Fe_3GeTe_2 single crystals by using Eq. (2).

Field direction	T_c (K)	Fit T range (K)	χ_0 (emu/mol)	C (emu K/mol)	θ_p (K)
$H \parallel c$	201.1	$240 \leqslant T \leqslant 300$	-4.25×10^{-3}	8.412	208.4
$H \parallel ab$	196.1	$240 \leqslant T \leqslant 300$	-1.38×10^{-2}	7.914	204.3

are in the divalent state. The positive Weiss temperatures for both directions suggest FM correlations in this material.

Figures 2(c) and 2(d) show magnetization as a function of effective magnetic field $\mu_0 H_{\rm eff}$ at different temperatures with $H \parallel c$ axis and $H \parallel ab$ plane, respectively. Here, $\mu_0 H_{\rm eff} = \mu_0(H - N_d M)$, where N_d is the demagnetization factor. A method devoted to calculating N_d in rectangular ferromagnetic prism was used, with details given in Ref. [34]. Saturation behavior is observed for both directions. The saturation fields at 2 K are $H_s^c = 0.4$ T for $H \parallel c$ axis and $H_s^{ab} = 3.5$ T for $H \parallel ab$ plane, which indicates the easy magnetization direction is the c axis. Moreover, the saturation magnetic moments at 2 K is $M_s^c = 4.1\mu_B$/formula for $H \parallel c$ axis, and $M_s^{ab} = 3.8\mu_B$/formula for $H \parallel ab$ plane. Similar magnetic anisotropy has also been observed in both frustrated and non-frustrated materials, such as $Pr_2Ir_2O_7$, Mn_3Sn, and $DyScO_3$. However, the microscopic mechanisms of the magnetization and its anisotropy differ [5,8,35]. To solve the above problem, detailed studies on magnetic structures with $H \parallel c$ axis and $H \parallel ab$ plane are still needed. In addition, field dependence of magnetizations along different directions in ab plane were also measured. This is because, from the perspective of crystal structure, it is not identical along different directions in the ab plane. However, no in-plane magnetic anisotropy was observed (see Fig. S2 in the supplementary material [33]). Consequently, the Hall resistivity anomaly discussed below with $I \parallel c$ axis is not related to the in-plane magnetization behavior.

Figure 3(a) exhibits the temperature dependence of the in-plane (ρ_{xx}) and out-of-plane (ρ_{zz}) resistivity. Both curves

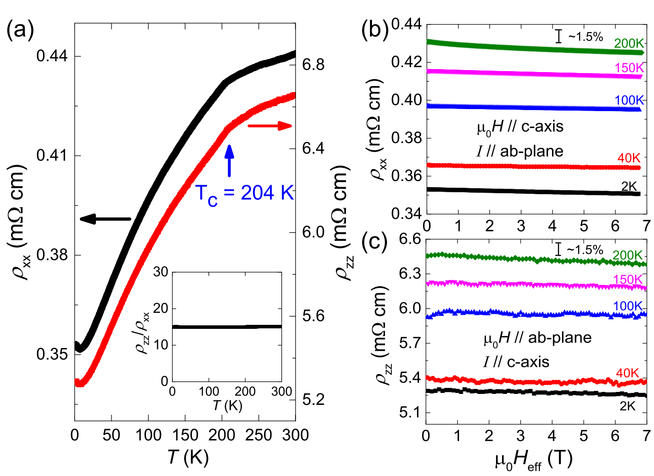

FIG. 3. (a) Temperature dependence of in-plane and out-of-plane resistivity for single crystal Fe_3GeTe_2. The inset shows that the resistivity anisotropy (ρ_{zz}/ρ_{xx}). (b), (c) Field dependence of in-plane and out-of-plane resistivities.

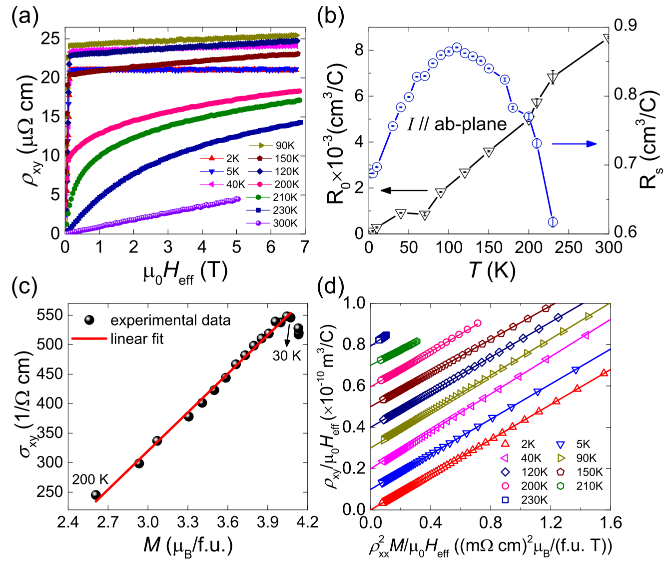

FIG. 4. (a) Field dependence of Hall resistivity with $I \parallel ab$ plane at indicated temperatures. (b) Temperature dependence of R_0 and R_s. Error bars indicate the standard error. (c) Hall conductivity plotted against the magnetization below T_c. (d) The $\rho_{xy}/\mu_0 H$ vs $\rho_{xx}^2 M/\mu_0 H$ curves at indicated temperatures. The curves have been offset subsequently by 1×10^{-11} m^3/C for clarity. Lines represent linear fits of data at different temperatures.

show metallic behavior with temperatures ranging from 2 to 300 K. For both directions, clear anomalies are found at ~204 K, corresponding well with T_c obtained from susceptibility measurements. The resistivity anisotropy ρ_{zz}/ρ_{xx} [inset in Fig. 3(a)] is as large as 15, indicating the system is quasi-2D. This conclusion is consistent with magnetic measurement results [31]. In addition, the ratio ρ_{zz}/ρ_{xx} is independent of temperature, which suggests that the in-plane and out-of-plane transports share the same scattering mechanism. Figures 3(b) and 3(c) exhibit the field dependence of ρ_{xx} and ρ_{zz} with current perpendicular to magnetic field, at the same time, parallel to the ab plane ($I \parallel ab$ plane) and c axis ($I \parallel c$ axis), respectively. Negative magnetoresistance behavior is presented with $I \parallel ab$ plane, indicating the spin-scattering is suppressed with increasing magnetic field. This phenomenon is common in ferromagnetic materials [36,37]. In addition, ρ_{xx} and ρ_{zz} are featureless and smaller than 1.5% at temperatures below T_c.

Figure 4(a) represents the field dependence of Hall resistivity ρ_{xy} at different temperatures with $I \parallel ab$ plane. The ρ_{xy} vs H curves share similar shape features with M vs H curves in Fig. 2(c). At low temperature (2 K), with increasing magnetic field, ρ_{xy} increases dramatically and saturates at 0.4 T, corresponding well with H_s^{ab} shown in Fig. 2(c). This result demonstrates that the magnetization dominates the AHE in Fe_3GeTe_2 with $I \parallel ab$ plane. The ordinary Hall coefficient R_0 and anomalous Hall coefficient R_s are separated by procedures described in Part III of the supplementary materials [33]. As shown in Fig. 4(b), R_0 is positive, indicating that the hole-type carrier is dominant in Fe_3GeTe_2. In addition, the value of R_0 increases steadily as the temperature increases, which indicates that the carrier density is sensitive to temperature. In contrast, R_s reaches a maximum at about 110 K, a temperature that deviates from Curie temperature. Similar temperature dependence of R_s is also observed in Ni and $La_{1-x}Sr_xMnO_3$ single crystals [38,39], and Mn_5Si_3 and Mn_5Ge_3 films [12,40]. Generally speaking, R_s exhibits a broad peak at $0.7T_c$–$0.8T_c$, and then decreases to zero in the paramagnetic state [18,41,42]. Furthermore, R_s is about two orders of magnitude larger than R_0. All the results above demonstrate that the AHE in Fe_3GeTe_2 with $I \parallel ab$ plane is conventional.

In general, the AHE can be depicted by conventional mechanisms [14–17]. Figure 4(c) shows Hall conductivity σ_{xy} plotted against magnetization M below T_c. It is distinct that the σ_{xy} of Fe_3GeTe_2 with $I \parallel ab$ plane is proportional to M. The relation is expected by K-L theory [14] and has also been observed in $La_{0.7}Sr_{0.3}MnO_3$ [39]. What is more, the linear-M Hall conductivity is also recognized as an evidence of the dissipationless nature of anomalous Hall current [43]. We note that the experimental data deviate from a linear fit below 30 K. This phenomenon is related to characteristic change of ρ_{xx} vs T curve at low temperature, which probably is caused by the scattering of conduction electrons due to magnetic impurities.

In Eq. (1), the anomalous Hall coefficient R_s is dependent on both magnetization M and resistivity ρ_{xx}, especially in materials exhibiting large magnetoresistance [44–48]. Consequently, the field dependence of resistivity should also be taken into consideration. Hence Eq. (1) can be written as

$$\rho_{xy} = R_0\mu_0 H + S_H \rho_{xx}^2 M, \tag{3}$$

where S_H is a material-specific scale factor [44,47]. The linear-M Hall conductivity indicates that Hall effect in Fe_3GeTe_2 with $I \parallel ab$ plane is expected to be explained by K-L theory. Equation (3) can be used to check the above conclusion over the whole temperature-magnetic-field range below T_c. Here the $\rho_{xy}/\mu_0 H$ vs $\rho_{xx}^2 M/\mu_0 H$ curves are shown in Fig. 4(d), which is motivated by a modification of Eq. (3): Dividing Eq. (3) by $\mu_0 H$ [47]. For clarity, the curves in Fig. 4(d) have been offset subsequently by 1×10^{-11} m^3/C. The good linear fits of data at different temperature confirm the conclusion that the AHE in Fe_3GeTe_2 with $I \parallel ab$ plane is best described by K-L theory.

Figure 5(a) shows the field dependence of the Hall resistivity ρ_{xz} at indicated temperatures with $I \parallel c$ axis. When $T > T_c$, the magnitude of ρ_{xz} increases in proportion to M, which indicates the spin-orbit coupling induced AHE dominates the Hall resistivity. Below T_c, ρ_{xz} increases linearly at low field, and then decreases gently and tends to saturate at high field, which shows striking contrast to M vs H curves along the ab plane [Fig. 2(d)].

Figure 5(b) exhibits a subset of field dependence of ρ_{xz} with $I \parallel ab$ plane. The solid lines are the fitting curves using the relation $\rho_{xz} = R_0\mu_0 H + S_H \rho_{zz}^2 M$ with the fitting parameter R_0 and S_H [45]. However, the estimates cannot explain the ρ_{xz} behavior at low field. Similar unconventional behavior has also been found in several magnetic frustrated materials [3,11], in which the Hall resistivity anomalies are attributed to the chiral effect induced by noncoplanar spin textures [4,5]. If we label the chiral contribution as ρ_{xz}^T, the Hall resistivity ρ_{xz} for Fe_3GeTe_2 with $I \parallel c$ axis can be depicted by an equation

$$\rho_{xz} = R_0\mu_0 H + S_H \rho_{zz}^2 M + \rho_{xz}^T. \tag{4}$$

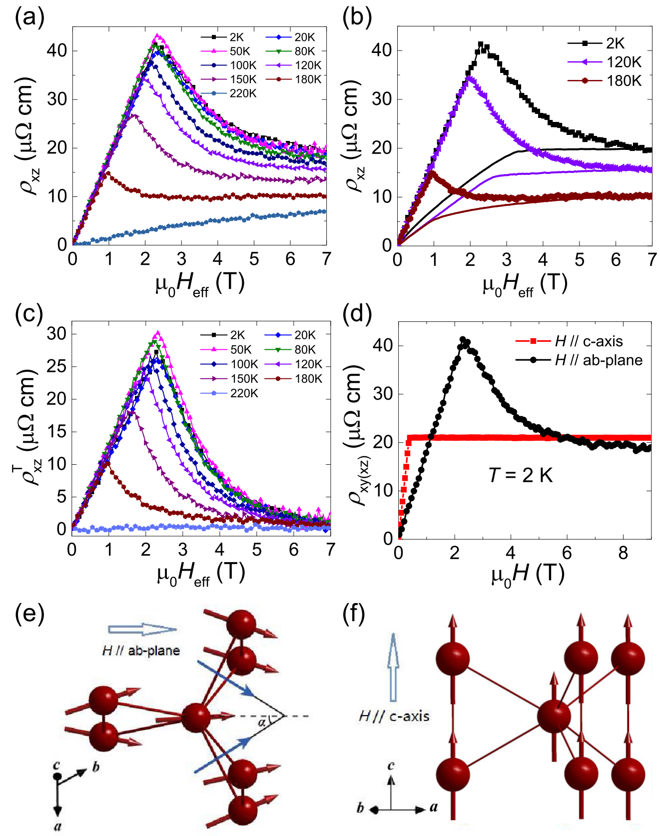

FIG. 5. (a) Field dependence of Hall resistivity with $I \parallel ab$ plane at indicated temperatures. (b) Field dependence of Hall resistivity with $I \parallel ab$ plane at indicated temperatures. For clarity, only a subset of data is shown. (c) Field dependence of the chiral effect to Hall resistivity ρ_{xz} at indicated temperatures. (d) The anisotropic field dependence of Hall resistivity ρ_{xy} and ρ_{xz} at 2 K with magnetic field along c axis and ab plane. (e), (f) Magnetic structure of the Fe sublattice during magnetization process with field along ab plane and c axis, respectively.

We note that the saturation behavior persists for a magnetic field up to 14 T (Fig. S4 in the supplementary material [33]). Accordingly, it is reasonable to propose that the chiral effect disappears at high field. Then ρ_{xz}^T can be obtained by subtracting the ordinary and anomalous part from the total Hall resistivity ρ_{xz} and shown in Fig. 5(c). Below T_c, ρ_{xz}^T shows a maximum at low field and decreases as the field increases. Figure 5(d) shows the field dependence of Hall resistivity at 2 K with $I \parallel ab$ plane and $I \parallel c$ axis. Obvious anisotropy is observed, indicating the different AHE mechanisms for the two directions.

In theory, the chiral effect is usually derived from noncoplanar spin textures and acts as a fictitious magnetic field in real space [20,26]. However, due to the compensation of fictitious magnetic field, the THE has only been observed in several magnetic frustrated materials [27,28]. From the perspective of the Fe_3GeTe_2 crystal structure, seven iron atoms share one vertex, forming three regular triangles that are parallel to c axis [Fig. 1(a)]. This peculiar structure prevents the compensation of the fictitious magnetic field, as discussed below.

Figure 5(e) shows the spin structure during the magnetization process with $H \parallel ab$ plane, and α is defined as the angle between the fictitious magnetic field $\boldsymbol{b}$ and external magnetic field H. Because the ab plane is a hard direction for Fe_3GeTe_2, the spins in iron atoms will flop from the easy axis (c axis) to the ab plane below T_c. During the spin-flop process, the spins are noncoplanar. As a result, the chiral effect appears and is represented as

$$\chi_{i,j,k} = S_i \cdot (S_j \times S_k), \tag{5}$$

where S_i, S_j, and S_k are three noncoplanar spins in a triangular formed by iron atoms [11]. The chiral effect acts as a fictitious magnetic field $\boldsymbol{b}$, which has a component $b\cos\alpha$ along direction of the external magnetic field. Consequently, a strong enhancement of ρ_{xz} is observed at low field. As the field increases further, the spins tend to align parallel because of the FM coupling along the ab plane, leading to the decrease of chiral effect and the fictitious magnetic field. As a result, ρ_{xz} decreases and tends to saturate at high field. Although there are no obvious anomalies in the ρ_{xz} vs H curves at high field (Fig. S4 in the supplementary material [33]), we still note that a small tilting angle of spins can also lead to the fictitious magnetic field in several materials such as $Nd_2Mo_2O_7$ [6]. Hence further investigations about the in-plane magnetic structure with $H \parallel ab$ plane are needed.

As the origin of the Hall resistivity anomaly at low field with $I \parallel c$ axis, one may consider the possibility that R_s becomes field dependent. As shown in Fig. S5 of the supplementary material [33] and Fig. 5(b), both the equation $\rho_{xz} = R_0\mu_0 H + S_A \rho_{zz} M$ (skew scattering) and $\rho_{xz} = R_0\mu_0 H + S_H \rho_{zz}^2 M$ (K-L theory or side jump) cannot give a good fit to ρ_{xz} vs H curves. Therefore, the anomalous Hall coefficient R_s seems insensitive to the magnetic field, and another contribution is expected to give an enhancement to ρ_{xz}. Although the spin chirality mechanism can properly explain the unconventional behavior of Hall resistivity with $H \parallel ab$ plane, other possibilities should also be taken into consideration because of the uncertainty of the magnetic structure at low field and the absence of theoretical calculation. For example, the skyrmion state or DM interaction may influence the Hall resistivity [4,46,49]. For the present material Fe_3GeTe_2, further investigations are still expected. In addition, the competition [32] of AFM and FM in this material has no reflection in the ρ_{xz} vs H curves. This is probably because, when the magnetic field is applied along ab plane, the spins in each single layer will flop from the easy axis (c axis) to the ab plane and give rise to a fictitious magnetic field $\boldsymbol{b}$ regardless the AFM or FM order.

Figure 5(f) shows the magnetic structure of iron lattice during magnetization process with $H \parallel c$ axis. Because the c axis is an easy axis of Fe_3GeTe_2, the spins are collinear and parallel with each other. Hence the chiral effect quenches, and only the conventional AHE appears.

According to reported data [31,32] and the present work, magnetic phase diagrams with $H \parallel c$ axis and $H \parallel ab$ plane were made and are shown in Fig. 6. For both directions with $T > T_c$, Fe_3GeTe_2 shows paramagnetic behavior and ordinary Hall effect in this temperature range. When $T < T_c$, the spins tend to arrange along the easy axis (c axis). Similar to a traditional ferromagnet, Fe_3GeTe_2 shows the anomalous Hall effect with $H \parallel c$ axis, as presented in Fig. 6(a). While for $H \parallel ab$ plane, as shown in Fig. 6(b), the triangular lattice formed by iron atoms is crossed by the magnetic field and the spins will flop from easy axis to the hard axis (ab plane). In the low-field region, the spins are noncoplanar during the spin-flop process. In this area, the THE shows up. As the field increases, the spins tend to become parallel, leading to the suppression of the THE.

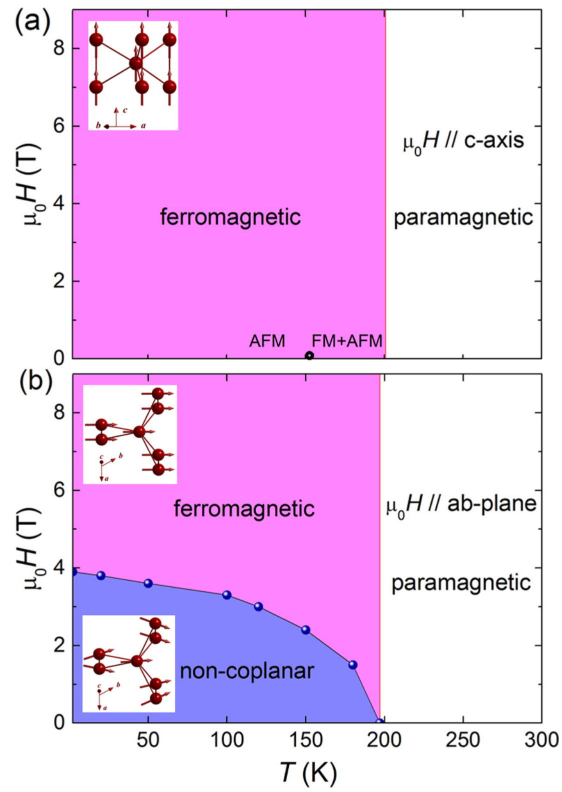

FIG. 6. Magnetic phase diagrams with (a) $H \parallel c$ axis and (b) $H \parallel ab$ plane. The circles denote the saturation fields H_s in M vs H curves.

According to Ref. [32], an AFM ground state was observed with magnetic moments parallel to the c axis at low ac magnetic field (3.9 Oe). However, the magnetic structure remains unknown with a large applied field along the c axis. Furthermore, the field dependence of M and ρ_{xy} show similar behavior as a ferromagnet. Consequently, we tend to define the magnetic phase to be FM with $H \parallel c$ axis below $T_c = 201.1$ K. More detailed investigations about magnetic structures with the field along the c axis and the ab plane are necessary.

IV. CONCLUSIONS

In summary, we prepared and investigated the transport properties of Fe_3GeTe_2 single crystals. Magnetization and resistivity measurements reveal an obvious anisotropy in this material. The conventional AHE shows up with $I \parallel ab$ plane. The Hall conductivity σ_{xy} is proportional to M, which conforms with the behavior expressed by K-L theory. On the other hand, an obvious enhancement of Hall resistivity shows up at low field with $I \parallel c$ axis and is likely explained by the chiral effect originating from the noncoplanar spin textures during the spin-flop process. For this reason, Fe_3GeTe_2 is expected to serve as an archetypal material to study the THE mechanism. Moreover, theoretical calculation and detailed experimental studies on magnetic structures below T_c with field along c axis and ab plane are desired to deepen our understanding of the origin of the anisotropic AHE.

ACKNOWLEDGMENTS

This work is supported by the National Key Research and Development Program of China (Grant No. 2016YFA0300404) and the NSFC (Grants No. U1432138, No. 11474288, No. 11574317, No. 21503233, No. U1532153, No. 11774352, and No. 11574322), the Major Program of Development Foundation of Hefei Center for Physical Science and Technology (Grant No. 2016FXZY001). Y.X. thanks the support of the Hundred Talents Program of the Chinese Academy of Sciences.

[1] N. Nagaosa, J. Sinova, S. Onoda, A. H. MacDonald, and N. P. Ong, Rev. Mod. Phys. **82**, 1539 (2010).

[2] C. M. Hurd, *The Hall Effect in Metals and Alloys* (Plenum Press, New York, 1972).

[3] H. Takatsu, S. Yonezawa, S. Fujimoto, and Y. Maeno, Phys. Rev. Lett. **105**, 137201 (2010).

[4] Y. Shiomi, M. Mochizuki, Y. Kaneko, and Y. Tokura, Phys. Rev. Lett. **108**, 056601 (2012).

[5] Y. Machida, S. Nakatsuji, Y. Maeno, T. Tayama, T. Sakakibara, and S. Onoda, Phys. Rev. Lett. **98**, 057203 (2007).

[6] Y. Taguchi, Y. Oohara, H. Yoshizawa, N. Nagaosa, and Y. Tokura, Science **291**, 2573 (2001).

[7] J. Kübler and C. Felser, Europhys. Lett. **108**, 67001 (2014).

[8] S. Nakatsuji, N. Kiyohara, and T. Higo, Nature (London) **527**, 212 (2015).

[9] N. Kiyohara, T. Tomita, and S. Nakatsuji, Phys. Rev. Appl. **5**, 064009 (2016).

[10] A. K. Nayak *et al.*, Sci. Adv. **2**, e1501870 (2016).

[11] B. Ueland *et al.*, Nat. Commun. **3**, 1067 (2012).

[12] C. Sürgers, G. Fischer, P. Winkel, and H. v. Löhneysen, Nat. Commun. **5**, 3400 (2014).

[13] T. Suzuki, R. Chisnell, A. Devarakonda, Y.-T. Liu, W. Feng, D. Xiao, J. W. Lynn, and J. G. Checkelsky, Nat. Phys. **12**, 1119 (2016).

[14] R. Karplus and J. Luttinger, Phys. Rev. **95**, 1154 (1954).

[15] J. Smit, Physica **21**, 877 (1955).

[16] J. Smit, Physica **24**, 39 (1958).

[17] L. Berger, Phys. Rev. B **2**, 4559 (1970).

[18] P. Matl, N. P. Ong, Y. F. Yan, Y. Q. Li, D. Studebaker, T. Baum, and G. Doubinina, Phys. Rev. B **57**, 10248 (1998).

[19] J. Ye, Y. B. Kim, A. J. Millis, B. I. Shraiman, P. Majumdar, and Z. Tešanović, Phys. Rev. Lett. **83**, 3737 (1999).

[20] T. Jungwirth, Q. Niu, and A. H. MacDonald, Phys. Rev. Lett. **88**, 207208 (2002).

[21] M. Onoda and N. Nagaosa, J. Phys. Soc. Jpn. **71**, 19 (2002).

[22] H. Chen, Q. Niu, and A. H. MacDonald, Phys. Rev. Lett. **112**, 017205 (2014).

[23] Y. Zhang, Y. Sun, H. Yang, J. Železný, S. P. P. Parkin, C. Felser, and B. Yan, Phys. Rev. B **95**, 075128 (2017).

[24] R. Moessner and A. P. Ramirez, Phys. Today **59**(2), 24 (2006).

[25] L. Balents, Nature (London) **464**, 199 (2010).

[26] N. Nagaosa, J. Phys. Soc. Jpn. **75**, 042001 (2006).

[27] I. Martin and C. D. Batista, Phys. Rev. Lett. **101**, 156402 (2008).

[28] Y. Akagi and Y. Motome, J. Phys. Soc. Jpn. **79**, 083711 (2010).

[29] H.-J. Deiseroth, K. Aleksandrov, C. Reiner, L. Kienle, and R. K. Kremer, Eur. J. Inorg. Chem. **2006**, 1561 (2006).

[30] A. F. May, S. Calder, C. Cantoni, H. Cao, and M. A. McGuire, Phys. Rev. B **93**, 014411 (2016).

[31] B. Chen, J. Yang, H. Wang, M. Imai, H. Ohta, C. Michioka, K. Yoshimura, and M. Fang, J. Phys. Soc. Jpn. **82**, 124711 (2013).

[32] J. Yi, H. Zhuang, Q. Zou, Z. Wu, G. Cao, S. Tang, S. A. Calder, P R. C. Kent, D. Mandrus, and Z. Gai, 2D Mater. **4**, 011005 (2017).

[33] See Supplemental Material at http://link.aps.org/supplemental/10.1103/PhysRevB.96.134428 for details of transport measurements, in-plane magnetization anisotropy measurements, the procedure of separation between R_0 and R_s, the field dependence of ρ_{xz} from 0 to 14 T, and ruling out the skew scattering mechanism.

[34] A. Aharoni, J. Appl. Phys. **83**, 3432 (1998).

[35] L. S. Wu *et al.*, Phys. Rev. B **96**, 144407 (2017).

[36] H. Yanagi, R. Kawamura, T. Kamiya, Y. Kamihara, M. Hirano, T. Nakamura, H. Osawa, and H. Hosono, Phys. Rev. B **77**, 224431 (2008).

[37] H. Y. Hwang, S.-W. Cheong, N. P. Ong, and B. Batlogg, Phys. Rev. Lett. **77**, 2041 (1996).

[38] J.-P. Jan, Helv. Phys. Acta **25**, 677 (1952).

[39] Y. Onose and Y. Tokura, Phys. Rev. B **73**, 174421 (2006).

[40] C. Zeng, Y. Yao, Q. Niu, and H. H. Weitering, Phys. Rev. Lett. **96**, 037204 (2006).

[41] K. Adachi and K. Ohkohchi, J. Phys. Soc. Jpn. **49**, 154 (1980).

[42] J. J. Rhyne, Phys. Rev. **172**, 523 (1968).

[43] W.-L. Lee, S. Watauchi, V. L. Miller, R. J. Cava, and N. P. Ong, Science **303**, 1647 (2004).

[44] M. Lee, Y. Onose, Y. Tokura, and N. P. Ong, Phys. Rev. B **75**, 172403 (2007).

[45] N. Kanazawa, Y. Onose, T. Arima, D. Okuyama, K. Ohoyama, S. Wakimoto, K. Kakurai, S. Ishiwata, and Y. Tokura, Phys. Rev. Lett. **106**, 156603 (2011).

[46] Y. Shiomi, S. Iguchi, and Y. Tokura, Phys. Rev. B **86**, 180404(R) (2012).

[47] S. Friedemann, M. Brando, W. J. Duncan, A. Neubauer, C. Pfleiderer, and F. M. Grosche, Phys. Rev. B **87**, 024410 (2013).

[48] Y. Li, N. Kanazawa, X. Z. Yu, A. Tsukazaki, M. Kawasaki, M. Ichikawa, X. F. Jin, F. Kagawa, and Y. Tokura, Phys. Rev. Lett. **110**, 117202 (2013).

[49] A. Neubauer, C. Pfleiderer, B. Binz, A. Rosch, R. Ritz, P. G. Niklowitz, and P. Böni, Phys. Rev. Lett. **102**, 186602 (2009).